Three-Dimensional Numerical Study of Impinging Water Jets in Runout Table Cooling Processes

MYUNG JONG CHO, BRIAN G. THOMAS, and PIL JONG LEE

Cooling from impinging water jets in runout table (ROT) processing depends on the fluid flow and depth of water accumulated in the water pool that forms on the surface of the moving steel strip. This effect is investigated with a three-dimensional (3-D) computational model of fluid flow, pressure, and free surface motion for realistic banks of nozzles within the flow rate region of the ROT process (2400 to 9200 L/min m^2). The volume of fluid (VOF) method with the high-resolution interface capturing (HRIC) scheme was implemented to handle the free surface flow of the water jet, and the k-ε model was used for turbulence. The governing equations are discretized by a second-order accurate scheme and solved with the computational fluid dynamics (CFD) code Fluent. The model was validated with experimental measurements of free-surface shape and hydraulic jump position for a single water jet impinging onto a moving surface that included turbulent flow and multiphase regions of mixed bubbles and water. For banks of water jets impinging onto the surface of the moving strip in a realistic ROT, the free surface shape, velocity, and pressure distributions have been calculated for various flow rates and surface widths. A deeper water pool is expected on the moving surface with increasing water flow rate and with increasing width. In addition, as the water pool height increases, the pressure variations on the moving surface below the water jets decrease. A simple relation to predict the water pool height from the water flow rate per unit area and strip width has been derived. The predictions agree well with both the 3-D calculations and measurements from water model experiments.

DOI: 10.1007/s11663-008-9160-8

I. INTRODUCTION

CONTROLLED cooling[1,2] from the impingement of water jets is used in many commercial processes to optimize the microstructure and properties of metal products. In the runout table (ROT) cooling process after hot rolling, steel producers have developed many new technologies[3–6] to lower production costs, to continuously improve product quality, and even to create new microstructures, in order to fulfill the increasing demands of customers. For example, to produce higher strength steel with less alloying elements, technology to increase the cooling rates is of growing interest.

Several technologies[6–9] to increase the cooling rate in the ROT have been recently developed. Ultrafast cooling technology[6,7] increases the conventional cooling rate of 30 °C/s to 80 °C/s, depending on the final thickness, to 300 °C/s on 4-mm-thick hot strip. An acceleration cooling technology[8,9] having more than 200 °C/s on 3-mm thickness makes it possible to increase the strength of steel or to achieve the same level of strength with a low carbon equivalent design. These technologies use larger flow rates than conventional cooling methods (such as spray or water column cooling), basically. In the ultrafast cooling, total water flow is well known as 17,000 L/min m[6] of cooling length. This corresponds to 9200 L/min m^2 assuming a 1.8-m width,[7] which is more than double the maximum flow rate for the conventional ROT cooling.[6]

The tools to develop these technologies include models of transient heat conduction in the moving strip.[10] They rely on heat-transfer coefficients between the impinging water jets and the strip surface, which are generally obtained from plant measurements.[10,11] The design of better cooling header systems requires knowledge of these heat-transfer coefficients as a function of the flow conditions, which depend on header configuration, nozzle geometry, spacing, height, flow rate, and other parameters. This knowledge is generally obtained from lab-scale experiments that must be further verified with full-scale prototypes in expensive plant experiments. Thus, there is a strong need for fundamentally-based tools to predict surface heat transfer in the real process.

There has been much previous work[12–16] on heat transfer from impinging jets (including free, confined, and submerged), based on experimental, analytical, and numerical studies. However, water impingement from multiple jets onto moving surfaces, and for the high flow rate conditions of real ROT cooling, has received much less attention. Specifically, these conditions involve the development of free gas-liquid surfaces and flow in the liquid pool above a high-temperature metal surface,

---

MYUNG JONG CHO and PIL JONG LEE, Principal Researchers, are with the Technical Research Lab., POSCO, Pohang City, 790-785, Korea. BRIAN G. THOMAS, W. Grafton and Lillian B. Wilkins Professor, is with the Department of Mechanical Science and Engineering, University of Illinois at Urbana-Champaign, Urbana, IL 61801. Contact e-mail: bgthomas@uiuc.edu

Manuscript submitted January 16, 2008.

where complex boiling, steam-layer development, and Leidenfrost effects occur. Heat transfer depends greatly on the details of the flow conditions, in addition to the surface temperature. A first step in the fundamental study of these complex phenomena is to quantify the location and depth of the free surface of the liquid pool. Recently, Gradeck *et al.*[17] studied the free surface of the water pool formed from a single water jet impinging on a moving surface. They investigated the water jump position both numerically and experimentally for conditions chosen to simulate a conventional ROT cooling process.

In this article, the flow pattern and free surface arising from multiple water jets impinging on a moving surface within the flow rate region of the ROT process has been simulated numerically and validated with measurements. Specifically, the effects of surface width and increasing flow rate have been investigated, and a general equation to predict the water pool depth has been developed.

II. ROT COOLING PROCESS

Figure 1 shows a typical ROT cooling process and close-up schematic of two adjacent water jets. As the steel strip moves from the hot rolling mill to the coiler, it passes under banks of cooling nozzles called "headers." Cooling water pours through each nozzle with diameter ϕ and forms a continuous stream of water that impinges onto the moving steel strip. It spreads over the moving surface. Similar cooling jets impinge from below the strip, not shown in Figure 1(c) for clarity. Heat transfer is influenced by the accumulation of a water pool on the moving strip. This is investigated by simulating the fluid flow pattern, velocity, and pressure distribution in this water pool and the shape of its free surface beneath a representative portion of the impinging water jets.

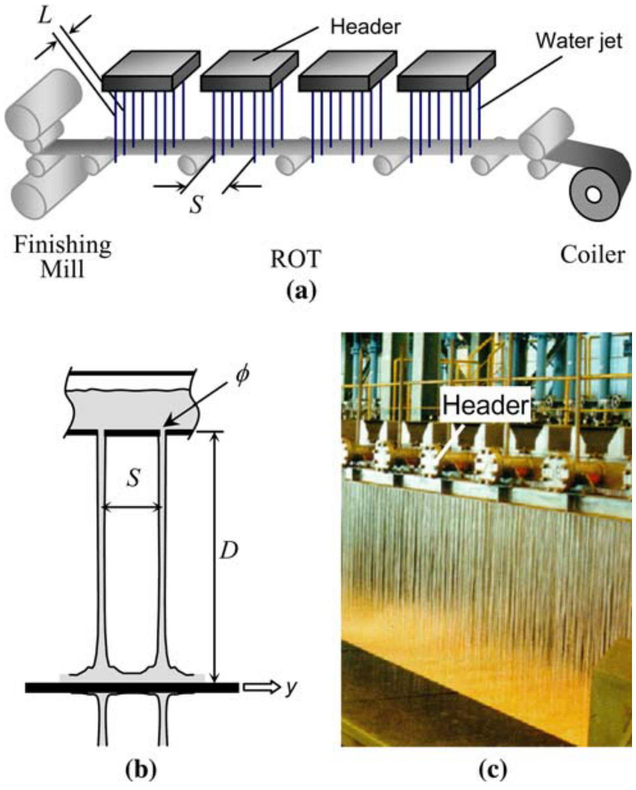

Fig. 1—Cooling process on the ROT.

III. NUMERICAL PROCEDURE

In this article, the standard conservation equations for steady-state incompressible mass and momentum conservation were calculated in a representative portion of the ROT, solving the standard Navier–Stokes equations in three dimensions. The inlet boundary condition at the entrance from each nozzle is fixed normal velocity V_j. The volume of fluid (VOF) model was adopted to calculate the shape of the free surface of the water pool due to the water jets impinging on the moving surface. An advanced interface capturing technique known as high-resolution interface capturing (HRIC) was selected for tracking the free surface with reduced numerical diffusion. This interface capture scheme can be used to solve the steady-state problem as well as transient ones. It was well known[18] that this scheme gives more efficient convergence to the final steady-state solution than other robust schemes based on transient solvers such as the donor-acceptor[19] or geometric reconstruction scheme.[20] A boundary condition of $\mathrm{VOF}_w = 1$ was assumed at each inlet plane, indicating that the nozzle exit was filled with cooling water.

The standard k-ε model was used for turbulence closure; the wall function approach was adopted at the surface of the moving strip, where normal velocity is zero; and the tangential boundary condition is the strip velocity. Pressure boundary conditions of 0 MPa gage are imposed on the non-nozzle portions of the top surface, where $\mathrm{VOF}_w = 0$ and on the free sides of the domain. The convection and diffusion terms of the governing equation were discretized using the second-order upwind scheme. The SIMPLE algorithm was employed to calculate the pressure. All computations were carried out using Fluent software (release 6.2.16).[21]

IV. VERIFICATION THROUGH SINGLE-JET TEST CASES

To test the accuracy of the present computational model, the experiment of Gradeck *et al.*[17] for a single water jet impinging onto a moving surface was simulated. As shown in Figure 2, the water jet issues from a 17-mm-diameter inlet located 60 mm above the moving surface, flows through a larger (22-mm) diameter development region, and impinges perpendicularly onto the moving surface. Figure 3 shows the 150 mm × 250 mm × 60 mm numerical grid of 117,000 cells and the boundary conditions employed. The first cells adjacent to the domain bottom were chosen in the region of $y^+ = 10$ to 40 (the lower limit for accurate wall function performance) to obtain a fine grid system near the moving surface. A uniform grid spacing of 5 mm in the *z* direction was adopted to facilitate capture of a sharp free surface.

The results of the calculated volume fraction of water (VOF_w) on the moving surface are compared in Figure 4 with the experimental hydraulic jump position for the case of strip velocity V_s = 1.5 m/s and jet velocity V_j = 1 m/s. In this figure, it was found that the edges of the hydraulic jump region were in good agreement with the contours of VOF_w = 0.8 and 0.2, respectively. In this comparison, it was thought that the range of VOF_w = 0.2 to 0.8 could approximately represent the bubble region in this highly turbulent, mixed flow problem. It was assumed that VOF_w = 0.2 was the proper value to define the free surface. In Figure 5, photographs[17] of the free surfaces of three cases with different surface moving speeds (V_s = 0.5, 1.0, and 1.5 m/s) were compared with the calculated

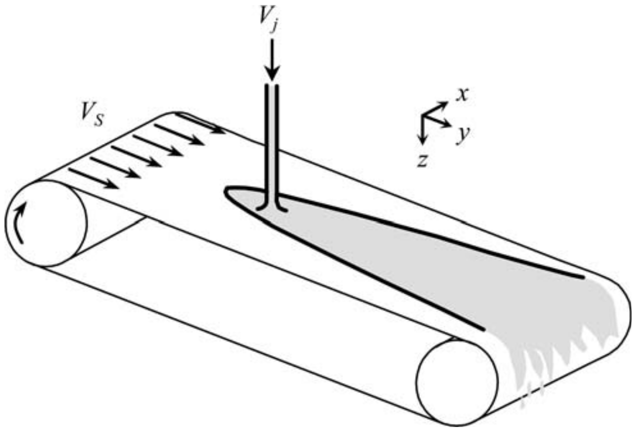

Fig. 2—Schematic view of the single water jet experiment[17] used for model verification.

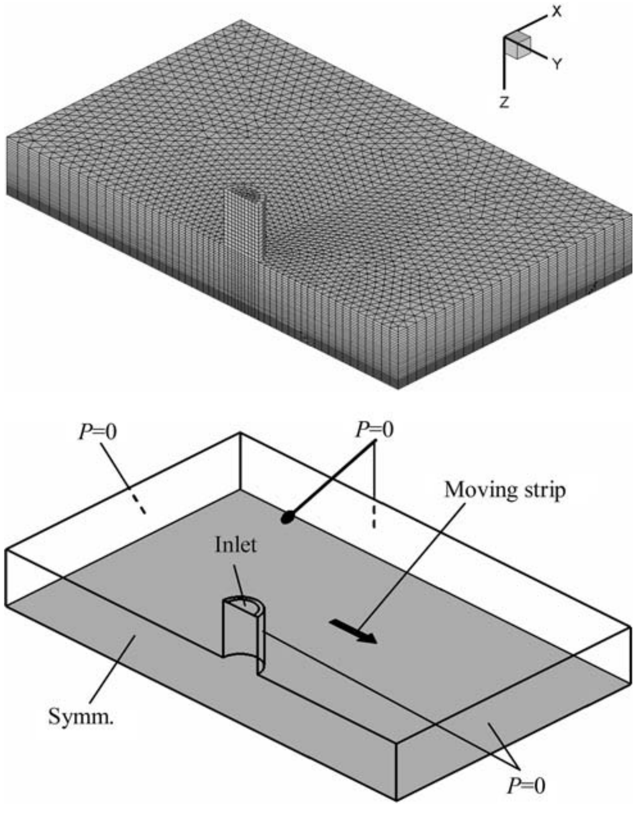

Fig. 3—Domain and boundary conditions for the single-water jet verification problem.

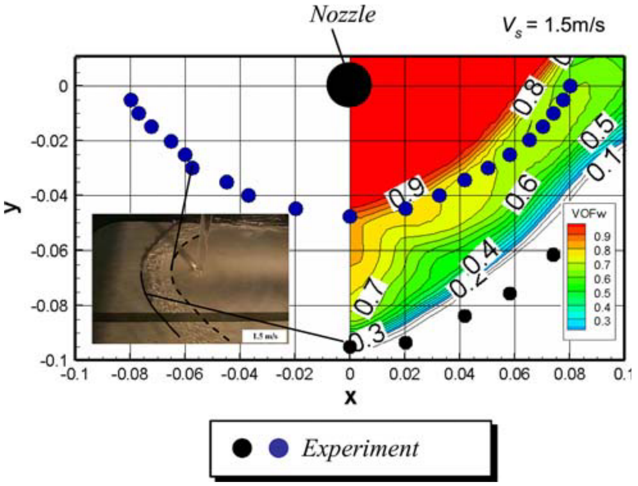

Fig. 4—Simulated volume fraction contours compared with measurement of hydraulic jump position and photo[17] (single water jet experiment).

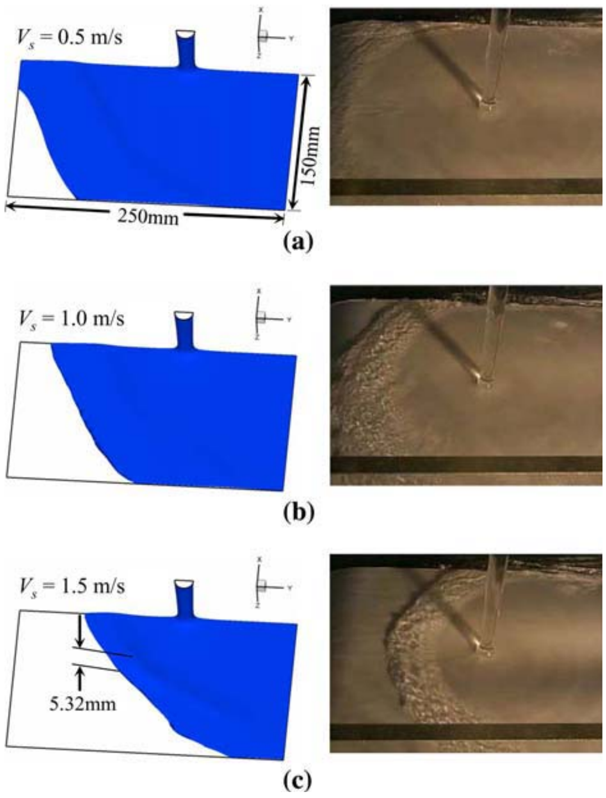

Fig. 5—Comparison of the free surface shape for the different surface velocities (3-D view).

isosurfaces of $\mathrm{VOF}_w = 0.2$. Increasing the speed naturally causes the hydraulic jump region to move closer to the jet, and to curve more. As shown in this figure, the calculated VOF_w isosurfaces agree reasonably well with the experimental free surface shapes. The predicted maximum water pool depths (in the hydraulic jump region) were 3.34, 3.64, and 5.32 mm for these three velocities, which appears again to match reasonably well with the measured results in Figure 5.

These findings show that the present computational model can quantitatively predict the shape of the free surface in an accumulated water pool on a moving surface, including the bubbles induced by the turbulent flow from an impinging water jet, with reasonable accuracy.

V. RESULTS

The validated model was then applied to simulate the flow, pressure, and free-surface shape of the accumulated pool in a real ROT, after steady-state conditions have been established. To approximate the flow pattern and profile that develops after in long banks of nozzles, a representative repeating portion of the process was chosen for the computational domain. It includes a double row of nozzles and part of the overflow region at the edge of the strip. This computational domain is a bank of nozzles near the middle of the ROT, which is far enough from the first and last nozzle banks that end effects can be ignored. Figure 6 shows the domain and boundary conditions, which take advantage of symmetry about the center plane. Because this domain typically repeats in the moving direction (y direction in Figure 6) to cover the entire cooling region of the real ROT process in Figure 1 (about 20 to 200 times), the flow velocities entering the upstream plane of the domain should roughly match those exiting the downstream plane. Therefore, the boundary condition for the two z-x planes was adopted to be periodic. The nozzles were arranged in a typical zigzag pattern with the same pitch ($S = L$), as shown in Figure 6. The velocity at the nozzle exit was determined according to the desired flow rate, the number of nozzles in the area, and their outlet diameter. The domain includes the entire height of the nozzle outlet above the moving strip, which allows the model to capture the acceleration of each falling jet and the corresponding decrease in jet area, which matches the Bernoulli equation. To ensure that the outlet boundary conditions do not affect the inner flow pattern, the domain was extended to include beyond where the water and air drain from the side. The grids were concentrated near the moving surface on the basis that the first cell near the wall has $y^+ = 10$ to 40. A total of 824,000 cells were arranged for the 300-mm-width case.

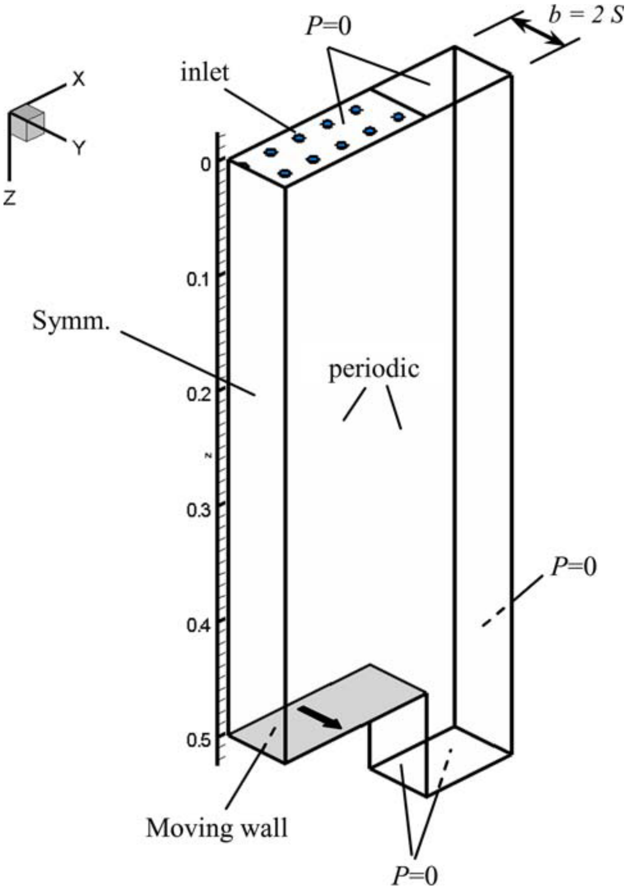

Fig. 6—ROT calculation domain and the associated boundary conditions.

A. *Conditions*

Water flow rates per unit area range from 2400 L/min m^2 (60 pct of the capacity of a conventional ROT cooling process) to a maximum flow rate of 9200 L/min m^2 for the high-flow rate ROT process.[6,7] Computations were carried out specifically for 2400, 4800, 7200, and 9200 L/min m^2. The nozzle diameter (ϕ), spacing (S), and pitch (L) were fixed at 8.3, 30, and 30 mm for all of the calculations, respectively. The speed of the moving surface (strip) was fixed at 10 m/s (600 mpm), and the height (D) of the nozzle above the moving surface was assumed to be 500 mm.

B. *Flow Rate Effect*

Figure 7 shows the calculated isosurfaces of $\mathrm{VOF}_w = 0.2$ for 300-mm width. In the case of 2400 L/min m^2, each impinging jet makes its own hydraulic jump. When the flow rate increases above 2400 L/min m^2, the hydraulic jump diminishes, making the surface smoother. In addition, the water pool height increases. When increasing the flow rate from 2400 to 9200 L/min m^2, the maximum height of the free surface ($\mathrm{VOF}_w = 0.2$) increases from 20 to 77 mm.

C. *Flow Pattern*

Figure 8 shows the typical flow pattern in the pool caused by the water jets, through tracers and velocity vectors for the 300 mm, 9200 L/min m^2 case. The water

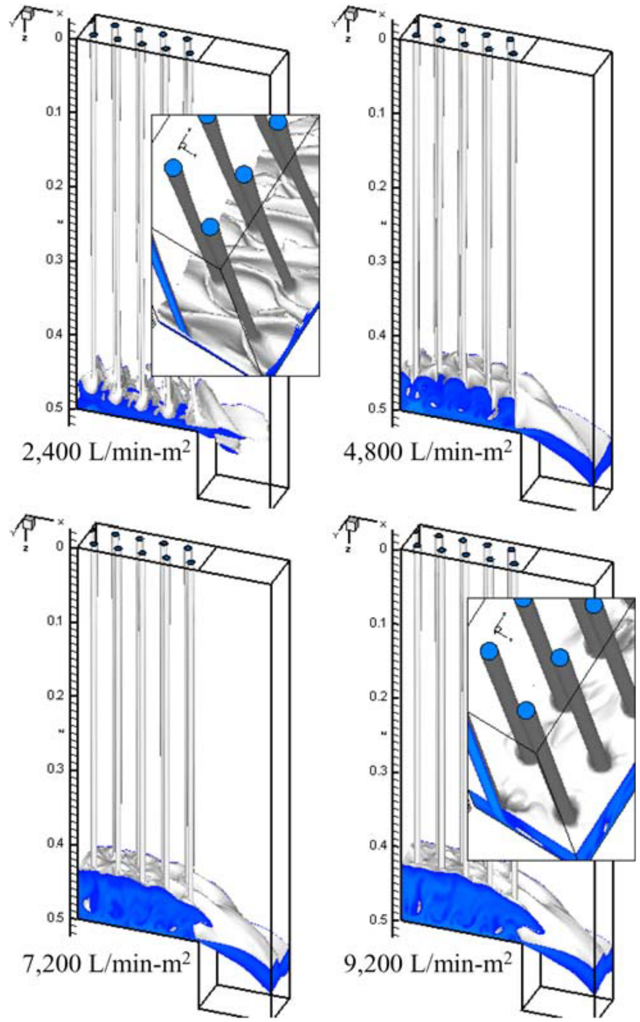

Fig. 7—Effect of flow rate on the calculated free surface shape (W = 300 mm).

columns all bend according to the bottom surface motion, causing flow recirculation and turbulence in the bottom of the pool. The bulk flow of water draining also bends the water columns, with increasing effect toward the edge of the strip. The air above the free surface (VOF_w = 0.2) is clearly shown to have high velocities and recirculation as well.

D. *Pressure*

Figures 9 and 10 present the calculated pressure contours and maximum pressure on the moving surface. Each jet creates a pressure peak that is stronger toward the strip edge, where the pool depth is less. From the classic Bernoulli equation, the maximum impact pressure of a free water jet should be proportional to the square of the nozzle exit velocity or the flow rate. However, Figure 10 shows that this effect saturates, and the maximum pressure does not increase much for flow rates over 7000 L/min m^2. This is because the deeper water pool absorbs the impact energy of the water jet.

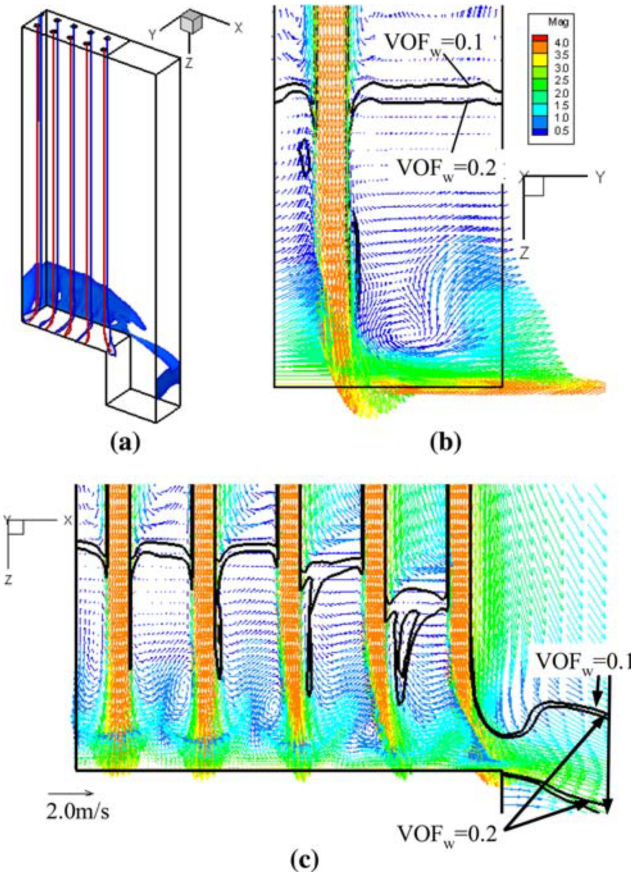

Fig. 8—Calculated results (w = 300 mm, 9200 L/min m^2): (a) vector tracers and the region of $\mathrm{VOF}_w > 0.2$, (b) velocity vectors and VOF_w contours at x = 30 mm, and (c) velocity vectors and VOF_w contours at y = 15 mm.

E. *Width Effect*

Next, simulations were performed for different surface widths (300, 600, 900, and 1200 mm) at constant flow rate (9200 L/min m^2). The predicted free surface of the standard 300-mm case is compared with the 1200-mm case in Figure 11. Although the overall shape of the water pool is nearly the same, increasing the width causes a deeper water pool height. Specifically, the pool height increases from 77 to 224 mm. This is because the total water flow increases in proportion to the width, for the same water flow rate per unit area. This flow must traverse a longer distance past more nozzles in a wide strip before it can reach and escape from the free edge.

The calculated maximum height of the volume fractions from each simulation is plotted in Figure 12. The effect of the free surface criterion (VOF_w = 0.2) is shown to be small, as the free surface height does not vary much for the range of VOF_w = 0.1 to 0.3. Volume fraction contours that are close together are generally indicative of a more reliable numerical solution.

The calculated pressure distributions for each width case are compared in Figure 13. The pressure can be divided into two components: the minimum or ''hydraulic'' pressure (P_h) and a pressure peak (ΔP), as shown in Figure 13. For 300-m width, a strong pressure peak is

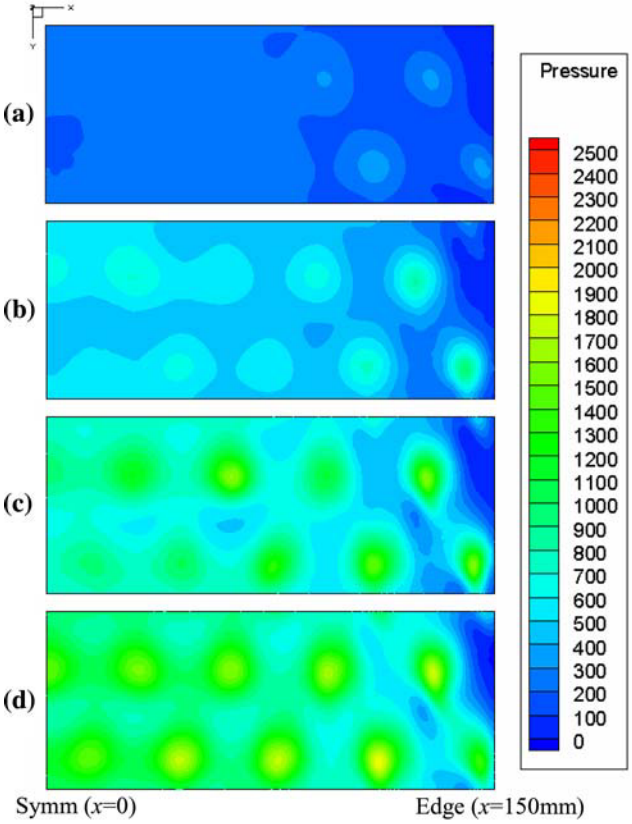

Fig. 9—Calculated pressure contours on the moving surface (W = 300 mm): (*a*) 2400 L/min m^2, (*b*) 4800 L/min m^2, (*c*) 7200 L/min m^2, and (*d*) 9200 L/min m^2.

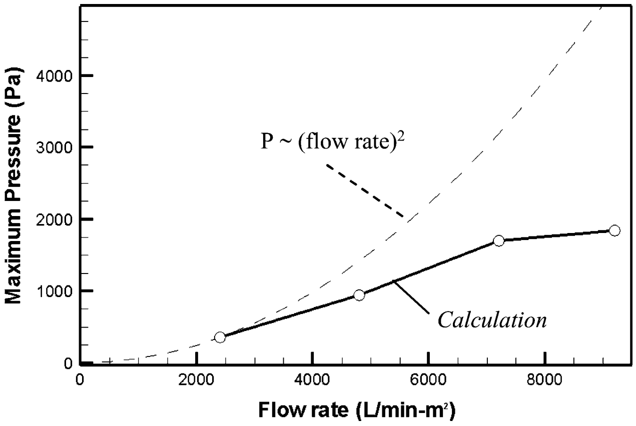

Fig. 10—Calculated maximum pressure on the moving surface (W = 300 mm).

found beneath each impinging jet. As the width increases, this pressure peak drops and disappears. However, the hydraulic pressure increases proportionately with the water pool depth, roughly according to P_h ($= \rho \cdot g \cdot H$).

In Figure 14, the hydraulic pressure and the maximum difference in pressures ΔP across the center region (x = 0 to 150 mm) are plotted for these four different

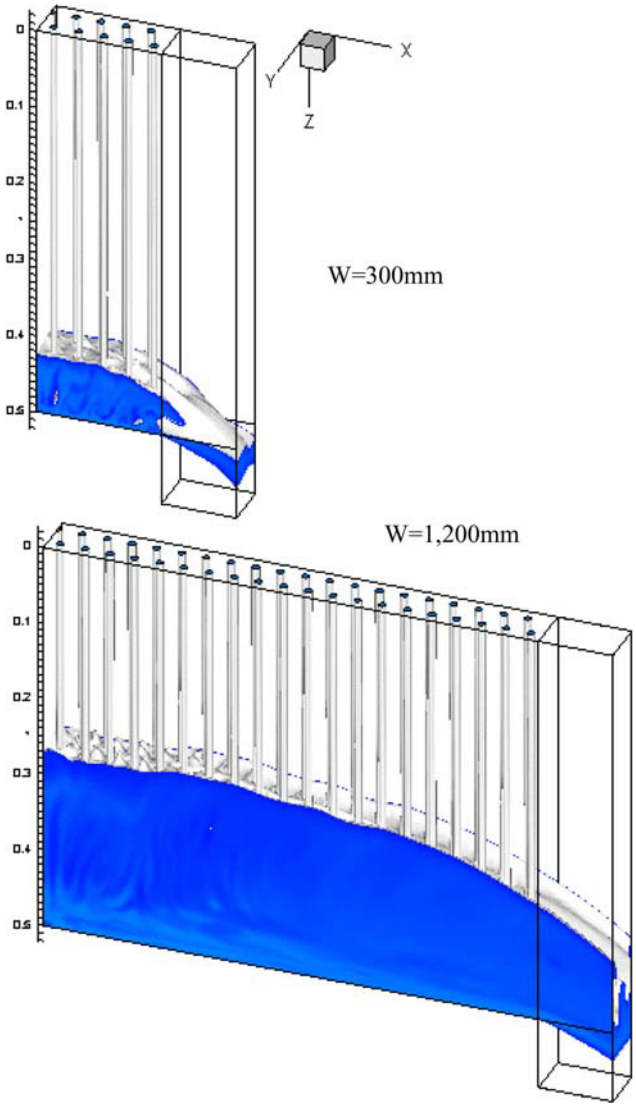

Fig. 11—Free surface shapes calculated for two different strip widths (9200 L/min m^2).

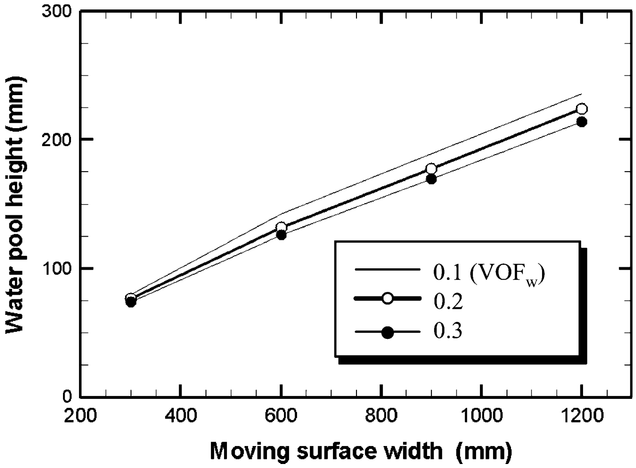

Fig. 12—Effect of strip width and volume fraction of water on pool height (9200 L/min m^2).

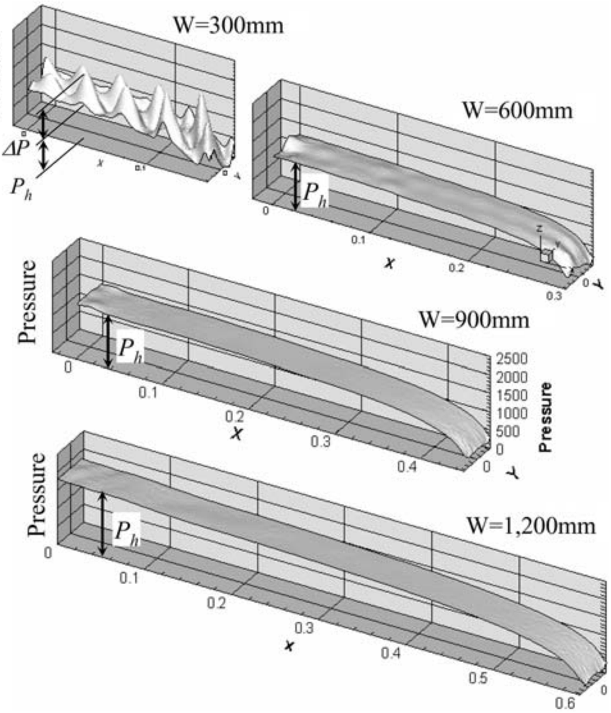

Fig. 13—Calculated pressure distributions on the moving surface (9200 L/min m^2).

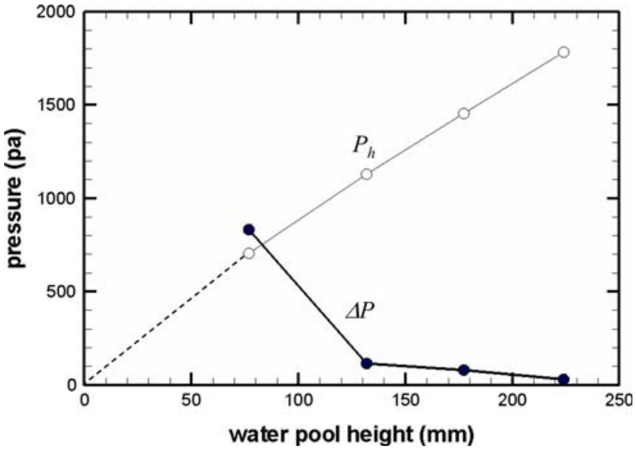

Fig. 14—Calculated pressure peak and hydraulic pressure on the moving surface (9200 L/min m^2).

width cases according to the water pool height. From this figure, it is clear that increasing the height of the water pool causes more of the impinging force of the water jet to be absorbed. Although the hydraulic pressure and the average pressure both increase, this effect causes the pressure difference to decrease.

VI. SIMPLE RELATION TO PREDICT POOL HEIGHT

The two open-channel flows over weirs sketched in Figure 15 have a similar draining mechanism with the

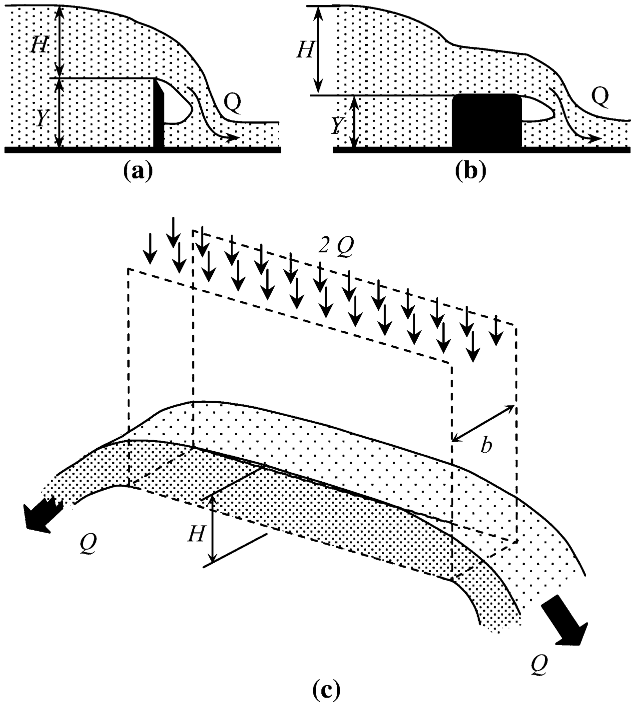

Fig. 15—Comparison of drain patterns in (*a*) open channel flow over a thin weir, (*b*) channel flow over thick weir, and (*c*) ROT.

present flow problem. Therefore, the following relation[22] between the total flow rate and water pool height for the open channel system was adopted to the present the flow problem:

$$H(\mathrm{m}) = C_d^{-2/3}\cdot b(\mathrm{m})^{-2/3}\cdot g^{-1/3}\cdot Q(\mathrm{m}^3/\mathrm{s})^{2/3} \qquad [1]$$

where

Q = total flow rate (m^3/s), as shown in Figure 15;
C_d = drag coefficient according to the weir shape;
b = weir length or water drain width (m), as shown in Figure 15;
g = 9.81 m/s^2; and
H = water pool height (m).

Tuning the unknown coefficient C_d with the calculated result for the 1200-mm case, C_d was calculated to be 0.275. Lenz[23] developed the C_d formula for the flow in Figure 15(b) as a function of H and Y. Specifically, decreasing the weir height Y causes a decrease in C_d. As an example, C_d drops from 0.544 to 0.275 as Y decreases from 3.7·H to 0.25·H. Because the present drain behavior is similar to Figure 15(b) with a small Y, the calculated C_d = 0.275 is thought to be reasonable.

The Eq. [1] was then rearranged into a practical prediction tool. First, Q and b are expressed in terms of plant process parameters:

$$Q(\mathrm{m}^3/\mathrm{s}) = q(\mathrm{L/min})/1000/60\cdot W(\mathrm{m})/2\cdot 2\ S(\mathrm{m})/L(\mathrm{m})/S(\mathrm{m}) \qquad [2]$$

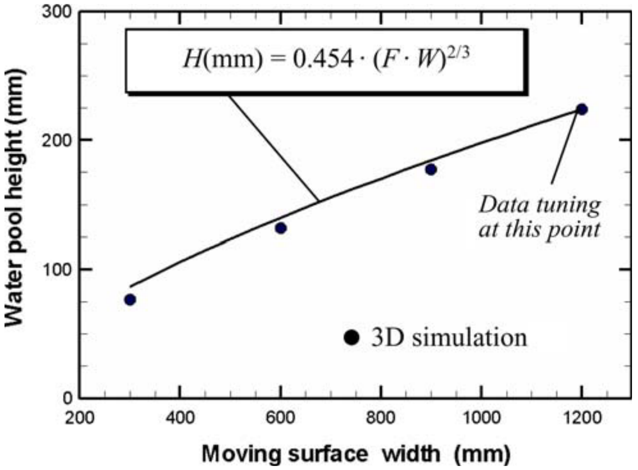

Fig. 16—Comparison of water pool height calculation (9200 L/min m^2).

$$b(\text{m}) = 2S(\text{m}) \qquad [3]$$

The flow rate per unit area, F, is defined as

$$F(\text{L/min m}^2) = q(\text{L/min})/L(\text{m})/S(\text{m}) \qquad [4]$$

where

q = flow rate per one nozzle (L/min),
W = width of moving surface (m),
L = spacing between nozzles in width direction (m), and
S = spacing between nozzles in moving (length) direction (m).

Inserting Eqs. [2] through [4] into Eq. [1], rearranging in terms of H, and combining C_d and g, gives

$$H(\text{mm}) = 0.454 \cdot \left[F(L/\text{min m}^2) \cdot W(\text{m})\right]^{2/3} \qquad [5]$$

or

$$H(\text{mm}) = 0.454 \times \left(\frac{q(\text{L/min}) \times W(\text{m})}{L(\text{m}) \times S(\text{m})}\right)^{2/3} \qquad [6]$$

The predictions of Eq. [5] are compared with those of the 3-D model in Figure 16. In this figure, very good agreement is found.

VII. EXPERIMENTAL VALIDATION OF SIMPLE RELATION

To verify the relation between flow rate and pool height given in Eqs. [5] and [6], a water model experiment shown in Figure 17, was considered. This model has a stationary bottom, while the current work was based on the bottom surface moving at 10 m/s. Thus, the effect of the bottom surface speed on the pool height was investigated first.

The free surfaces (VOF$_w$ = 0.2) of a new stationary-bottom simulation (9200 L/min m^2) and the corresponding moving case (10 m/s) are compared in Figure 18. The dips around the water columns of the moving surface case are elongated toward both the surface moving direction and the edge, whereas the dips in the stationary case elongate straight toward the edge, as shown in Figure 18(a). The maximum water pool heights of stationary cases are just slightly greater than those of the moving cases (86 mm *vs* 77 mm for 300 mm and 232 mm *vs* 224 mm for 1200 mm). This difference of less than 9 mm caused by the surface speed is not very significant relative to the natural variations in the surface profile caused by the turbulent flow.

Next, the predictions of the empirical equation were compared with the measurements of the water pool height in the water model experiment, for two different

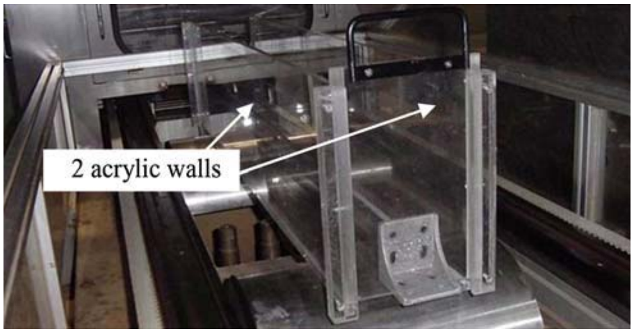

Fig. 17—Water pool height experiment.

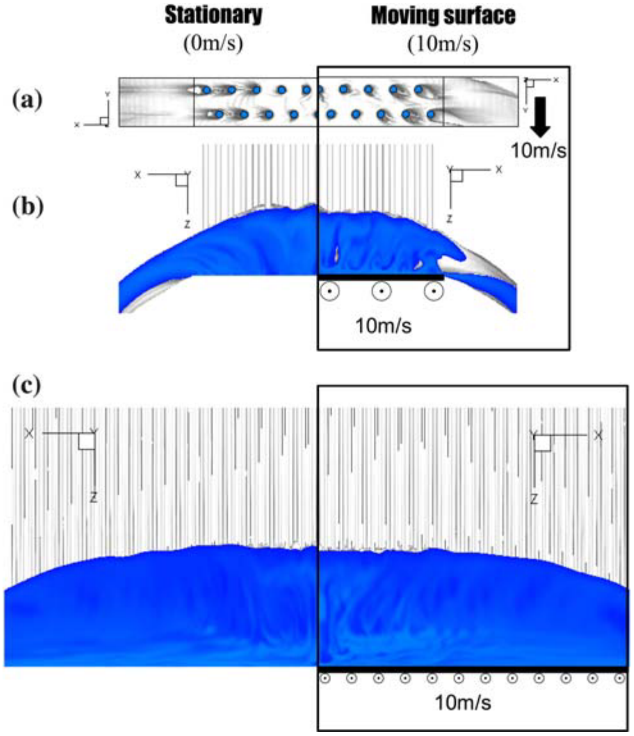

Fig. 18—Water pool height comparison between stationary and moving surface: (*a*) W = 300 mm (top view), (*b*) W = 300 mm (front view), and (*c*) W = 1200 mm.

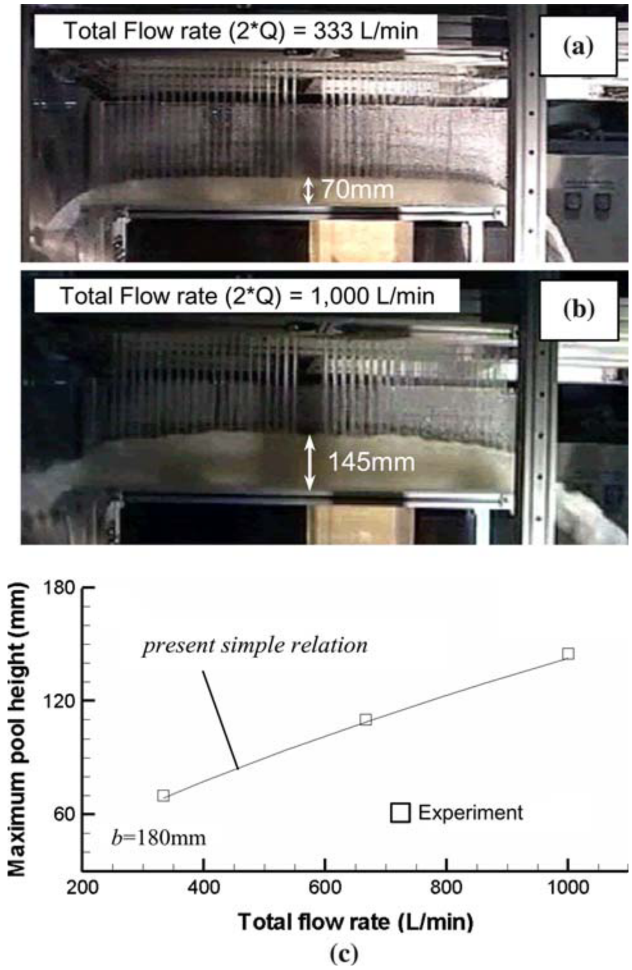

Fig. 19—Comparison of water pool height.

flow rates. Figures 19(a) and (b) show photos of experiments for a total flow rate = 333 L/min (1545 L/min m^2) and 1000 L/min (4635 L/min m^2). These photos reconfirm that the water pool forms and contains bubbles. The water pool decreases in height toward the opening at the side. This is the same tendency as those shown by the model predictions (Figure 18). In Figure 19(c), the experiment water pool height was compared with that of Eq. [6]. Variations in the free surface height of 1 to 5 mm are caused by each water jet, as seen in both the water experiments and in the computations. Within the uncertainty of these natural variations, the relation developed in this work between the pool height, flow rate, and width agrees very well with the experiment.

VIII. IMPLICATIONS FOR HEAT TRANSFER

The previous sections have presented a model for predicting the water pool depth that has been validated with experimental measurements. This provides an indication of the ability of the model to predict flow and pressure variations in the water pool, which is a crucial step in predicting heat transfer at the water/strip interface. This work is also useful in providing an initial indication of heat transfer in real processes. Generally, a deeper water pool would be expected to increase heat transfer, owing to the increased water available to remove heat. However, for very deep water pools, for the same flow conditions, heat transfer may decrease, owing to the increased uniformity of the pressure and flow fields, which makes steam removal more difficult. This has important practical implications: for example, increasing the strip width at high water flow rates likely causes the heat transfer to decrease due to the water pool height increase. Without accounting for this, laboratory experiments may differ from the real plant.

Comparisons of heat transfer between the top and bottom of the strip confirms that the relationship between the pool depth and heat transfer is not simple, as many other phenomena are involved. Thus, much further work is needed: a comprehensive fundamental model of water vaporization, steam layer development, and boiling heat transfer is being developed as future work.

IX. CONCLUSIONS

In this article, impinging water jets on a moving surface has been numerically studied to investigate flow behavior in a realistic range of ROT processes. The 3-D k-ε Reynolds averaged Navier–Stokes model features a second-order accurate discretization and the VOF method with the HRIC scheme to handle the free surface flow and was implemented in Fluent 6.2.16. The model accurately predicted the free-surface shape in a verification problem of a single impinging water jet experiment using a volume fraction of 0.2 to define the free surface.

The velocities, free surface shape, and pressure on the moving surface were calculated for various flow rates and strip widths. The results show that increasing the flow rate over 2400 L/min m^2 causes a deep water pool to accumulate on the moving surface. The water pool depth increases with increasing strip width and increasing flow rate. It was also found that the pressure peak below each water jet decreases as the water pool height increases.

Based on the similarity in drainage flow behavior of the present problem with open-channel flow over a dam, a simple equation was derived to predict the pool height from the water flow rate, nozzle spacings, and strip width. Pool height predictions using the simple equation agree well with those of the water model experiments as well as the 3-D computations. The flow results have important implications for heat transfer in ROT processes, which are discussed briefly in preparation for further work.

ACKNOWLEDGMENT

The authors express their sincere gratitude to Professor Gradeck for his help in providing the single water jet experimental data for the verification.

REFERENCES

1. Z.D. Liu and I.V. Samarasekera: *J. Iron Steel Res. Int.*, 2004, vol. 11, pp. 15–23.
2. J. Sengupta, B.G. Thomas, and M.A. Wells: *Metall. Mater. Trans. A*, 2005, vol. 36A, pp. 187–204.
3. Arvedi and Siemens VAI Team: *Steel Times Int.*, 2006, vol. 30, p. 23.
4. J.A. Kromhout, A.A. Kamperman, M. Kick, and F. Mensonides: *Ironmaking and Steelmaking*, 2006, vol. 33, pp. 362–66.
5. K. Sekiguchi, Y. Anbe, and H. Imanari: *Trans. Institute of Electrical Engineers of Japan*, 2004, vol. 124D, pp. 190–95.
6. J.C. Herman: *Ironmaking and Steelmaking*, 2001, vol. 28, pp. 159–63.
7. A. Lucas, P. Simon, G. Bourdon, J.C. Herman, P. Riche, J. Neutjens, and P. Harlet: *Steel Res. Int.*, 2004, vol. 75, pp. 139–46.
8. F. Akio and O. Kazuo: *JFE Techn. Rep.*, 2005, No. 5, pp. 10–15.
9. F. Akio, I. Sadanori, H. Yoshimich, M. Toru, M. Yoichi, and I. Shozo: *EP Patent Application* EP 1 210 993 A1, 2002.
10. C.G. Sun, H.N. Han, J.K. Lee, Y.S. Jin, and S.M. Hwang: *ISIJ Int.*, 2002, vol. 42, pp. 392–400.
11. M.A. Smith and K. Weinzierl: *Iron Steel Technol.*, 2007, vol. 4, pp. 108–18.
12. B.W. Web and C.F. Ma: *Adv. Heat Transfer*, 1995, vol. 26, pp. 105–217.
13. J.H. Lienhard: *Ann. Rev. Heat Transfer*, 1995, pp. 199–270.
14. S.V. Garimella: *Ann. Rev. Heat Transfer*, 2000, pp. 413–94.
15. A.T. Hauksson, D. Fraser, V. Prodanovic, and I.V. Samarasekera: *Ironmaking and Steelmaking*, 2004, vol. . 31, pp. 51–56.
16. Z.D. Liu, D. Fraser, and I.V. Samarasekera: *Can. Metall. Q.*, 2002, vol. 41, pp. 63–74.
17. M. Gradeck, A. Kouachi, A. Dani, D. Arnoult, and J.L. Borean: *Exp. Therm. Fluid Sci.*, 2006, vol. 30, pp. 193–201.
18. Fluent Inc.: *Tips Tricks Fluent MAT Enews*, 2005, Mar.
19. C.W. Hirt and B.D. Nichols: *J. Comput. Phys.*, 1981, vol. 39, pp. 201–25.
20. D.L. Youngs: *Numerical Methods for Fluid Dynamics*, Academic, New York, NY, 1982.
21. Fluent 6.3 Manual, Ansys Inc., Lebanon, NH, 2007.
22. F.M. White: *Fluid Mechanics*, 5th ed., McGraw-Hill, New York, NY, 2003, pp. 724–26.
23. A.T. Lenz: *ASCE Trans.*, 1943, vol. 108, pp. 759–802.